

Learning of Causal Observable Functions for Koopman-DFL Lifting Linearization of Nonlinear Controlled Systems and Its Application to Excavation Automation*

Nicholas S. Selby¹ and H. Harry Asada²

Abstract—Effective and causal observable functions for low-order lifting linearization of nonlinear controlled systems are learned from data by using neural networks. While Koopman operator theory allows us to represent a nonlinear system as a linear system in an infinite-dimensional space of observables, exact linearization is guaranteed only for autonomous systems with no input, and finding effective observable functions for approximation with a low-order linear system remains an open question. Dual Faceted Linearization uses a set of effective observables for low-order lifting linearization, but the method requires knowledge of the physical structure of the nonlinear system. Here, a data-driven method is presented for generating a set of nonlinear observable functions that can accurately approximate a nonlinear control system to a low-order linear control system. A caveat in using data of measured variables as observables is that the measured variables may contain input to the system, which incurs a causality contradiction when lifting the system, i.e. taking derivatives of the observables. The current work presents a method for eliminating such anti-causal components of the observables and lifting the system using only causal observables. The method is applied to excavation automation, a complex nonlinear dynamical system, to obtain a low-order lifted linear model for control design.

I. INTRODUCTION

There is a growing need in the construction and mining industries for excavation automation. Various technologies are being developed for operating excavators autonomously with increased productivity and fuel efficiency [1]. The worldwide shortage of skilled operators to operate excavators is a major driver behind the development of intelligent excavators for performing earth-moving tasks [2].

Excavation is a highly nonlinear process where soil and rocks interact with the bucket of an excavator in a complex manner (see Fig. 1). While terramechanics models have been studied for many decades, their validity is limited due to the difficulty in identifying the numerous parameters of mechanistic models. Data-driven methods have recently been introduced to autonomous excavation for capturing complex nonlinearities [3]–[6], yet the nonlinear models are still too complex to use, in particular, for real-time control.

Lifting linearization is a methodology for representing a nonlinear dynamical system with a linear dynamic model in a high dimensional space. Underpinned by Koopman operator theory, nonlinear systems represented with supernumerary

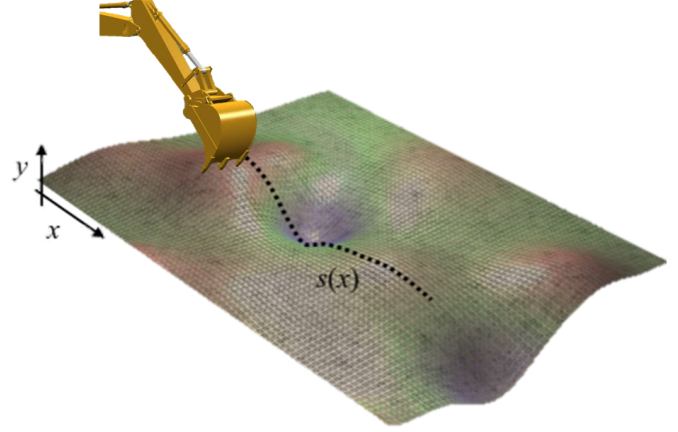


Fig. 1. Autonomous excavation simulation.

state variables behave more linearly in the lifted space. The method has recently been applied to various robotics and automation challenges, including active learning [7], soft robotics [8], human-robot interaction [9], power systems [10], and mission planning [11]. More broadly, deep learning has proven a valuable tool in a variety of lifting linearization techniques [12]–[15].

The original Koopman Operator has two major limitations:

- 1) The theory is applicable only to dynamical systems with no exogenous input, i.e. autonomous systems, and
- 2) The exact linear representation requires an infinite-dimensional space, except for a restricted class of systems.

Any extension to non-autonomous, finite-dimensional systems is no longer exact, but an approximation. Various methods for truncating the system with a finite-dimensional space have been reported. Among others, the eigendecomposition of the lifted system allows us to represent the system at desirable accuracy and granularity while providing useful insights into the system [16]. Furthermore, the extended Dynamic Mode Decomposition (EDMD) is completely data-driven, providing a practical tool for complex nonlinear system representation. These methods, however, need a set of observables, i.e. output variables, which are nonlinear functions of independent state variables. It is still an open question how to find an effective set of observable functions.

One of the key challenges in the lifting linearization of nonlinear systems with exogenous input is causality. If observable functions are functions of both state variables and input variables, we cannot use such observables for lifting

*This material is based upon work supported by National Science Foundation Grant NSF-CMMI 2021625.

¹Nicholas S. Selby is a PhD Candidate in the Department of Electrical Engineering and Computer Science at the Massachusetts Institute of Technology, 77 Massachusetts Ave, Cambridge, MA, USA nselby@mit.edu

²H. Harry Asada is with the Faculty of the Department of Mechanical Engineering at the Massachusetts Institute of Technology asada@mit.edu

the system. Lifting entails computing time derivatives of the observables and, thereby, the dynamic equations inevitably include the time derivative of input. In discrete formulation, this means the use of future input. Including these input terms, the time-evolution of the observables turns out not to be causal. If one measures a set of observables from a nonlinear system that is subject to control inputs and uses the observables for lifting the system, they may end up with a non-causal dynamical system.

In Dual-Faceted Linearization (DFL)—another approach to lifting linearization—this causality issue has been analyzed based on physical system modeling theory [17]. In DFL, the propagation of inputs across the nonlinear dynamical system can be tracked, and their effect upon all observables, called auxiliary variables, can be localized. Assuming that inputs are linearly involved in observables, a method has been established for eliminating the input-dependent component from each observable and lifting the dynamics by using the remaining input-free observables. In the Koopman-based lifting linearization, too, it is assumed that the system is input-affine in order to eliminate the input-dependent components from observable functions, so that a causal dynamic model can be obtained [18].

Lifting linearization is a powerful methodology for tackling a broad spectrum of nonlinear problems, in particular, excavation process modeling and control. However, two critical challenges have not yet been fully solved:

- 1) Finding an effective set of observables that can approximate a nonlinear system in a low-dimensional lifted space, and
- 2) Finding causal observables that are uncorrelated with inputs.

The current work presents a method for achieving these two; a low-dimensional, causal, lifting linear model is obtained from experimental data. Neural networks are used for finding such a set of causal, effective observables through learning.

In the following, we summarize a basic formulation of lifting linearization in § II. We present the learning method for obtaining an effective set of observables in § III. First, we deal with nonlinear controlled systems where all measured observables are not affected by inputs. Then, the method is extended for physical observables that may be functions of inputs. Simple numerical examples are discussed for validating the proposed method in § IV, and we apply it to excavation process modeling in § V.

II. BACKGROUND

This section summarizes background knowledge for readability. More details can be found in [17], [19].

A. Koopman Operator Theory

First proposed in 1931 by Koopman [19], Koopman operator theory originally modeled only autonomous systems, and the operator mapped the nonlinear dynamics only onto an infinite-dimensional linear space. Later techniques expanded the use of the operator for nonautonomous systems

[20] and developed methods for approximating the infinite-dimensional mapping with a computationally feasible, finite-dimensional space [21]–[23].

Let the discrete-time dynamics of a nonlinear, autonomous system with state $x_t \in \mathbb{R}^l$ at time t be given by:

$$x_{t+1} = f(x_t) \quad (1)$$

Furthermore, define a vector of nonlinear observables of the state, $\eta_t \in \mathbb{R}^m$, given by:

$$\eta_t = g(x_t) \quad (2)$$

The Koopman operator, \mathcal{K} , is linear and infinite-dimensional and applies to observable functions:

$$\mathcal{K}_f g = g \circ f \quad (3)$$

where \circ represents the composition operator.

B. Dual-Faceted Linearization (DFL)

Despite the use of Koopman operators to provide a lifting linearization for autonomous systems, the theory provides no method by which to select an effective set of observables. Because it is infeasible to compute the infinite-dimensional space with finite computational resources, the choice of which observables to use is very important. DFL uses a particular class of observables that are determined based on physical modeling theory and bond graphs [17]. Those observables, called auxiliary variables, are physically meaningful, and may be measured physically. Furthermore, causality analysis of the method allows us to examine how exogenous inputs propagate the system and influence specific auxiliary variables. Using those variables with no input influence, one can obtain a lifted system that is causal. Alternatively, input-dependent variables can be “laundered” into causal variables.

Consider the discrete-time dynamics of a nonlinear, nonautonomous system with input $u_t \in \mathbb{R}^n$ at time t given by:

$$x_{t+1} = f(x_t, u_t) \quad (4)$$

Assuming that the system is a lumped-parameter system with integral causality, we can choose nonlinear observables $\eta_t = g(x_t) \in \mathbb{R}^m$ to augment the system state and construct a linear representation of the system dynamics:

$$x_{t+1} = A_x x_t + A_\eta \eta_t + B_x u_t \quad (5)$$

where $A_x \in \mathbb{R}^{l \times l}$, $A_\eta \in \mathbb{R}^{l \times m}$, and $B_x \in \mathbb{R}^{l \times n}$ are fixed matrix coefficients determined by the physical structure of the system. This part of the state evolution is exact.

We approximate the η -dynamics using a second equation:

$$\eta_{t+1} = H_x x_t + H_\eta \eta_t + H_u u_t + r_{\eta_{t+1}} \quad (6)$$

where $H_x \in \mathbb{R}^{m \times l}$, $H_\eta \in \mathbb{R}^{m \times m}$, and $H_u \in \mathbb{R}^{m \times n}$ are fixed matrix coefficients and $r_{\eta_{t+1}} \in \mathbb{R}^m$ is a residual. Unlike A_x , A_η , and B_x , which are determined from the physical structure of the system, H_x , H_η , and H_u must be regressed from data. For brevity, define overall coefficient matrices $A \triangleq (A_x, A_\eta, B_x) \in \mathbb{R}^{l \times p}$ and $H \triangleq (H_x, H_\eta, H_u) \in \mathbb{R}^{m \times p}$ and an overall datum vector $\xi_t \triangleq (x_t^\top, \eta_t^\top, u_t^\top)^\top \in \mathbb{R}^p$ where $p = l + m + n$. By applying a negative discrete-time shift operator

T_{-1} to (6), H can be optimized to minimize the mean squared error of predicting η_{n+1} :

$$\begin{aligned} H^o &= \arg \min_H E [|H\xi_t - \eta_t|^2] \\ &= E [\eta_t \xi_{t-1}^T] (E [\xi_{t-1} \xi_{t-1}^T])^{-1} \end{aligned} \quad (7)$$

where $E[\cdot]$ is the expectation operator. Assuming that the system is persistently excited and that there is no state feedback, i.e., u_t is not collinear with x_t , there is a unique solution, H^o .

The original nonlinear dynamics f can now be modeled using the dual faceted linear dynamics:

$$\begin{cases} x_{t+1} = A\xi_t \\ \eta_{t+1} \approx H\xi_t \\ \eta_0 = g(x_0) \end{cases} \quad (8)$$

Practical benefits of using DFL as a tool to model systems include:

- Augmented state feedback can be used to better inform controllers [24].
- Linear observer design is enabled for augmented state feedback.
- Model-predictive control is convex [16].
- Because DFL is based in physical modelling theory, augmented state systems may be measurable, and dynamics may have physical intuition [25].

For these reasons, DFL has proven to be a valuable tool in modeling nonlinear systems. However, DFL requires knowledge of the structure of the physical system. Furthermore, many systems contain no obvious, measurable observables with which to augment the state, and there is no guarantee that, when they do exist, physically meaningful observables make the best choices for augmenting the system state.

C. Machine Learning for Linear Latent Spaces

Koopman operator theory and DFL are closely related to learned latent-space dynamic modeling techniques. They all involve constructing a nonlinear representation of the original state, then using a model to evolve the new “observables” through time. In Koopman operator theory and DFL, the dynamic model is constrained to be linear. Recently, much work has been done to explore applying deep learning techniques to Koopman operators.

Abraham and Murphey [7] presented an active learning strategy for robotic systems that extended observables, g , from Koopman operator theory to include the control input, u_t , as well as the system state, x_t . Their algorithm trains a neural network to approximate an optimal g . In each epoch, they recompute a finite-dimensional matrix approximation of the Koopman operator \mathcal{K} , but because g is a function of both x_t and u_t , regressing such a matrix requires knowing u_{t+1} in addition to x_{t+1} . To solve this causality problem, they propose a novel control synthesis algorithm to predict u_{t+1} , somewhat constraining the options for controlling the system.

Han *et al.* [26] also proposed using a neural network that approximates an optimal lifting function g . At the end of each epoch, after feeding x_{t-1} forward through g , they solve a

least squares optimization problem to regress a modified H^o where $H_x = 0$, then use the learned model to backpropagate the error $E [|g(x_t) - H^o \xi_{t-1}|_F]$ plus a penalty on the norms of the components of H^o . Because they do not track the evolution of the state, x , directly, they must simultaneously learn an additional matrix to approximate g^{-1} .

Other work in learned latent spaces for lifting1 linearizations leverages neural networks to approximate functions similar to Koopman’s observables in reinforcement learning [15], sampling-based motion planning [13], Kalman filtering [14], and partially observable Markov decision process [12] paradigms. However, these works all learn linearizations A and H that are time- or state-dependent, further reducing the long-term robustness of the linear model and giving up the benefits of provably convex optimal control.

D. Anticausal Observables

Most lifting linearization techniques, including Koopman operator theory and DFL, require that the lifting observables be control input-independent, i.e. $\eta = g(x)$. If auxiliary variables depend on the control input, u , i.e. $\eta = g(x, u)$, then the time derivative of η includes the time derivative of the control input:

$$\dot{\eta}(x, u) = \frac{\partial \eta}{\partial x} \dot{x} + \frac{\partial \eta}{\partial u} \dot{u} \quad (9)$$

In order to avoid problems with causality, most methods explicitly avoid augmenting the system state with control input-dependent variables. There are two common techniques used.

The first solution to the causality problem is to include a state-feedback control law in the model [7], [26]. By constraining the control input to be a known function of state, the system becomes effectively autonomous, and the original formulation of Koopman operator theory applies. This works for regulators, but no exogenous input is allowed.

The second solution to the causality problem is to assume that the auxiliary variables are linear in u [17], [18], [27]:

$$\eta(x, u) = \eta^*(x) + Du \quad (10)$$

where η^* is exclusively state-dependent and D is a fixed matrix coefficient of u .

Although predicting future values of $\eta(x, u)$ remains impossible without a control law, this formulation allows for the modeling of the evolution of $\eta^*(x)$. The auxiliary state equation can be rewritten:

$$\dot{\eta}^* = H_x^* x + H_\eta^* \eta + H_u^* u + r_{\dot{\eta}^*} \quad (11)$$

where $r_{\dot{\eta}^*}$ is a residual.

Substituting (10) into (11) yields:

$$\dot{\eta}^* = H_x^* x + H_\eta^* \eta^* + (H_u^* + H_\eta^* D) u + r_{\dot{\eta}^*} \quad (12)$$

which is a causal, augmented state dynamic equation.

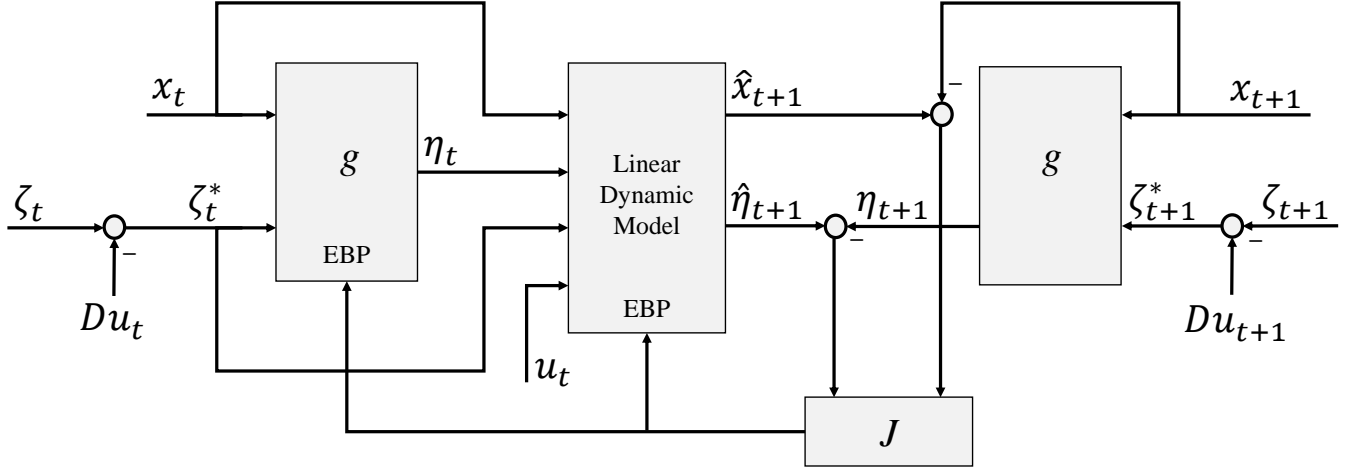


Fig. 2. Block diagram of the learned lifting linearization algorithm. The loss, J , is used to tune the weights of neural network, g , and linear dynamic model matrices A and H via error backpropagation (EBP). Note that both instances of g are equivalent to each other for all time t .

III. MODELING ALGORITHM

Fig. 2 shows the overview of the modeling algorithm. First, we assume all state variables are accessible and sufficient data for training are attainable. All state variables are fed into the left neural network, g , to produce a set of synthetic observables, η_t , to be learned. The state x_t , observables η_t , and input u_t are fed into the linear dynamic model parameterized by matrices A and H . The linear model produces predicted state \hat{x}_{t+1} and predicted observables $\hat{\eta}_{t+1}$. The predicted state and observables are compared to their ground truth values, x_{t+1} and $\eta_{t+1} = g(x_{t+1}; \theta)$, respectively. The right neural network in the figure is a twin copy of the left neural network, sharing parameters θ .

The squared error of the predicted state and observables, J , is used for updating the Linear Dynamic Model with respect to parameters A and H and the neural network weights. The update of these parameters is computed via error backpropagation (EBP).

The causality analysis involved in the DFL modeling allows us to examine whether observables, called auxiliary variables, are functions of state alone or include inputs. If some auxiliary variables are causal, having no dependence on control input, they can be added to the state for lifting the dynamics. Let ζ_t^* represent causal auxiliary variables. As shown in Fig. 2, the causal observables can be fed into the neural network, so that the synthetic auxiliary variables η_t can be produced from richer data. Note that the ground truth η_{t+1} , too, can be produced in response to not only state x_{t+1} but also ζ_{t+1}^* . The tunable parameter space of the neural network is expanded with the use of the causal auxiliary variables.

In case physically measurable auxiliary variables are functions of both state and input, such input-dependent auxiliary variables cannot be used in their original form for lifting the dynamics. It is necessary to filter out the input components from the observables. Fig. 2 also shows a simple filter to eliminate the effect of input from those variables, ζ_t , as discussed in § III-B.

A. Discrete-Time Learned Lifting Linearization

Consider the discrete-time dynamic system from (4). Let g be a neural network defined by randomly initialized parameters θ to generate synthetic observables:

$$\eta_t^\theta = g(x_t; \theta) \quad (13)$$

Define a datum vector $\xi_t^\theta \triangleq (x_t^\top, \eta_t^{\theta\top}, u_t^\top)^\top$. Let $A \in \mathbb{R}^{l \times p}$ and $H \in \mathbb{R}^{m \times p}$ be matrix coefficients modeling the state and augmented state transition dynamics, respectively. We override (8) to include residuals in the original and augmented state dynamic equations:

$$\begin{cases} x_{t+1} = A\xi_t^\theta + r_{x_{t+1}}^\theta \\ \eta_{t+1}^\theta = H\xi_t^\theta + r_{\eta_{t+1}}^\theta \\ \eta_0^\theta = g(x_0; \theta) \end{cases} \quad (14)$$

Given observation data of x_t , x_{t-1} , and u_{t-1} , we synthesize observations of the augmented state, $\eta_t^\theta = g(x_t; \theta)$ and $\eta_{t-1}^\theta = g(x_{t-1}; \theta)$, and assemble datum vectors ξ_{t-1}^θ .

By applying the discrete-time shift operator T_{-1} to (14) and rearranging, we can compute a residual for each observation:

$$\begin{cases} r_{x_t}^\theta = x_t - A\xi_{t-1}^\theta \\ r_{\eta_t}^\theta = g(x_t; \theta) - H\xi_{t-1}^\theta \end{cases} \quad (15)$$

We define a quadratic loss function, $J_t(\theta, A, H)$, used to train the model:

$$J_t(\theta, A, H) \triangleq r_t^{\theta\top} Q r_t^\theta \quad (16)$$

where Q is a symmetric matrix coefficient and r_t^θ is a total residual given by

$$r_t^\theta \triangleq (r_{x_t}^{\theta\top}, r_{\eta_t}^{\theta\top})^\top \quad (17)$$

Model parameter matrices A and H , as well as the parameters of the neural network, θ , are computed by solving the following optimization problem:

$$\theta^o, A^o, H^o = \arg \min_{\theta, A, H} \mathbb{E}[J_t(\theta, A, H)] \quad (18)$$

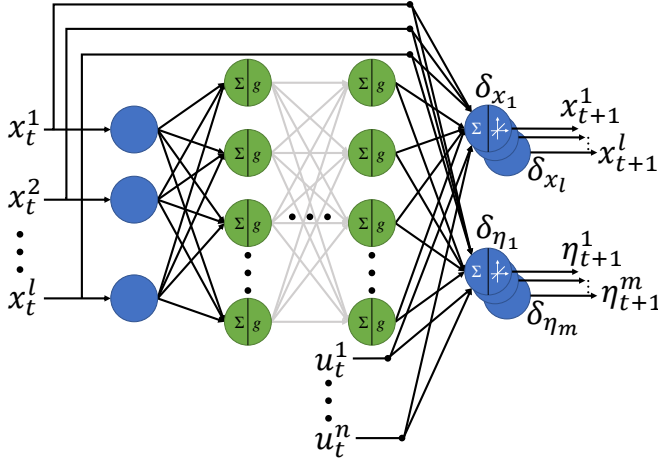


Fig. 3. Diagram of the neural network and linear dynamic model to compute x_{t+1} and η_{t+1} given x_t and u_t . With abuse of notation, we hereafter include ζ^* in x .

There are two approaches to obtaining the optimal parameters θ^o , A^o , and H^o . One is based on least squares estimation combined with a gradient-based method, and the other is solely based on gradient-based optimization.

1) *Least Squares Estimate*: Equation (18) can be reduced to:

$$\begin{aligned} \theta^o, A^o, H^o &= \arg \min_{\theta} [\min_{A, H} [E [J_t(\theta, A, H)]] \\ &= \arg \min_{\theta} E [J_t(\theta; A^o(\theta), H^o(\theta))] \end{aligned} \quad (19)$$

where $A^o(\theta)$ and $H^o(\theta)$ are the optimal coefficient matrices that minimize the squared error for a given parameter of the neural net, θ . For $Q = I$:

$$\begin{cases} A^o(\theta) = E [x_t \xi_{t-1}^{\theta \top}] \left(E [\xi_{t-1}^{\theta} \xi_{t-1}^{\theta \top}] \right)^{-1} \\ H^o(\theta) = E [g(x_t; \theta) \xi_{t-1}^{\theta \top}] \left(E [\xi_{t-1}^{\theta} \xi_{t-1}^{\theta \top}] \right)^{-1} \end{cases} \quad (20)$$

The optimization of the neural network parameter, θ , can be performed by using an error backpropagation algorithm. The cost functional $J_t(\theta; A^o(\theta), H^o(\theta))$, however, is highly complex; the partial derivatives of this cost functional with respect to θ are computationally expensive. Although $J_t(\theta; A^o(\theta), H^o(\theta))$ has been optimized in terms of A and H , the overall computation may be more complex. A remedy is to split the optimization into the least squares estimate of the linear dynamic model and the neural network tuning for generating the synthetic observables, η . These two can be computed sequentially and repeatedly multiple times, that is, a Bootstrap method. While computing the linear dynamic model using least squares, the neural net is fixed. While the neural net is being trained, the linear dynamic model is fixed. Namely, matrices A and H are kept constant, which makes the error backpropagation computation simpler.

2) *Gradient-Based Approach*: An alternative is to treat the linear dynamic model as another layer of the neural network and apply the error backpropagation algorithm through the extended network. Since the evolution of state, x , and synthetic observables, η , is linear, both can be represented with a

single layer of the network with a linear activation function. Fig. 3 shows the network structure. The linear dynamic model is the output layer of the augmented neural network. The δ -values associated with the final layer units can be computed directly from the cost:

$$\begin{cases} \delta_{x_i} = -\frac{\partial J_t}{\partial x_i} & i = 1, \dots, l \\ \delta_{\eta_j} = -\frac{\partial J_t}{\partial \eta_j} & j = 1, \dots, m \end{cases} \quad (21)$$

where the activation function is linear with unity slope. Simply backpropagating these δ -values, the parameters of the neural network, θ , can be trained.

The least squares estimate approach entails a centralized process with a large batch size for computing $A^o(\theta)$ and $H^o(\theta)$ in (20). In contrast, in the gradient-based approach, no batch processing is required, because mini-batch processing will be sufficient.

B. Extension to Anticausal Observables

As discussed in [17], augmenting the state with physical observables is often useful. Because this learned lifting linearization is data-driven, augmenting the state, x , with control-independent, physical observables is trivial. However, as reviewed in § II, if the augmented state is dependent on the control input, the augmented system dynamics may become anticausal. Consider a vector of physical observables, $\zeta(x, u)$, suspected of including a dependence on u . As in [17], [18], and [27], assume that this dependence is linear:

$$\zeta(x, u) = \zeta^*(x) + Du \quad (22)$$

where $\zeta^*(x)$ is exclusively a function of state and D is a fixed matrix coefficient of u . Because $\zeta^*(x)$ is uncorrelated with the control input, $E[\zeta^*(x)u^{\top}] = 0$. Therefore, multiplying (22) by u^{\top} and taking the expectation yields:

$$E[\zeta(x, u)u^{\top}] = DE[uu^{\top}] \quad (23)$$

Given observations of $\zeta(x, u)$ and u , computing D becomes a least-squares linear regression:

$$\hat{D} = E[\zeta(x, u)u^{\top}] E[uu^{\top}]^{-1} \quad (24)$$

Before training the learned lifting linearization model in (14), we preprocess the data to “clean” the physical observables from any linear dependence on u via

$$\zeta^*(x_t) = \zeta(x_t, u_t) - \hat{D}u_t \quad (25)$$

for each observation, t .

Then, we augment the DFL model to include $\zeta^*(x)$. We override (13):

$$\eta_t^{\theta} = g((\zeta^{*\top}(x_t), x_t^{\top})^{\top}) \quad (26)$$

and follow the same training procedure described above to tune g , A , and H using (18).

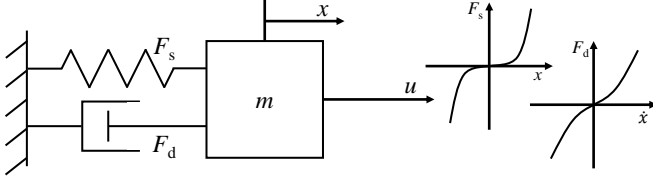


Fig. 4. Diagram of the toy problem system. F_s and F_d are forces acting on the mass by a nonlinear spring and damper, respectively; u is the control input; and x is the linear position.

IV. TOY PROBLEM

The modeling algorithm in § III is implemented in PyTorch [28] on a laptop running Ubuntu 18.04.5 LTS. The codebase is hosted as a git repository at [29].

We test the learned lifting linearization algorithm on the nonlinear mass-spring-damper illustrated in Fig. 4 with unity mass, $F_s = 0.2x + 2x^3$, and $F_d = 3\text{sgn}(\dot{x})x^2$. We generate 100 5s trajectories at 20Hz with initial conditions and control inputs drawn from uniform random distributions. The state, x , consists of the linear position of the mass, x , and the linear velocity of the mass, \dot{x} .

The neural network, g , approximating the optimal synthetic observables, η , is a fully connected network of two linear input neurons ($l = 2$); four hidden layers, each with 256 ReLU neurons; and 7 linear output neurons ($l + m = 7$). This neural net creates 5 synthetic observables ($m = 5$). Before training, the data are randomly divided 80-20 into a training set and a validation set. The neural network, g , and the linear model consisting of A and H are trained in batches of 50 input-output pairs using an Adam optimizer [30] with $\alpha = 10^{-4}$, $\beta_1 = 0.9$, $\beta_2 = 0.999$, and $\epsilon = 10^{-8}$. The quadratic cost parameter $Q = I$. Before each training epoch, the learned lifting linearization model is evaluated using the validation dataset without backpropagating the loss. Training continues until the validation loss begins to increase.

We benchmark the learned lifting linearization algorithm against the Koopman-based method. Using the same data from the training and validation sets described above, 35 observables using polynomial basis functions are created for the Koopman observables. Therefore, the domain of the Koopman dynamic model has a dimensionality of 35, whereas the domain of the learned lifting linearization dynamic model has a dimensionality of only 5, a much lower dimension. For Koopman, we used the data to compute least squares estimates of the matrix coefficients of observables and control inputs.

After training the learned lifting linearization model and computing the Koopman model, we simulated both models given a zero initial condition and a square wave input trajectory. The modeled state trajectory is compared against the ground truth in Fig. 5. The learned lifting linearization model outperforms the Koopman model despite the significantly lower dimensionality. The integrated absolute errors of the Koopman and learned lifting linearization models are 17.4 and 16.2, respectively. Note that the fidelity of the Koopman operator model is sensitive to hyperparameters. As discussed

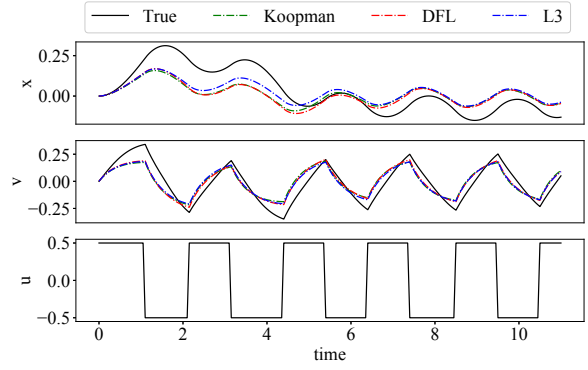


Fig. 5. Results of simulation predicting the position and velocity of the mass given a zero initial condition and a square wave input. The solid black line indicates the true trajectory. The dashed green line indicates the trajectory predicted by the Koopman model. The dashed red line indicates the trajectory predicted by the DFL model. The dashed blue line indicates the trajectory predicted by the learned lifting linearization (L3) model.

in [8], without L1 regularization, high-dimensional Koopman models quickly overfit to the training data.

We also benchmark the learned lifting linearization algorithm against the dual faceted linearization. DFL augments the state using physical observables $\eta = (F_s, F_d)^T$, which are only 2. The lifted space dimension is therefore only $2+2 = 4$. The state transition model, A , is determined from the physical structure of the model shown in Fig. 4. This state equation is exact. On the other hand, the augmented state transition model, H , must be computed as a least squares estimate problem using (7).

In Fig. 5, the learned lifting linearization model is also compared to the DFL model. The former has a slight advantage: in addition to penalizing nonlinearities in the state transition equation, the cost function of the learned lifting linearization in (16) also penalizes nonlinearities in the augmented state transition equation. The integrated absolute error of the DFL model is 17.1, slightly worse than the learned lifting linearization model.

We also use the toy problem to compare the least squares estimator and gradient-based approaches to learning g , A , and H . We implement both algorithms and compare the results in Table I. The results are numerically approximate, but simulations of the two methods reveal that the LSE approach results in far greater error. We hypothesize that the reason for the differing results comes from the inclusion of $r_{\eta_i}^\theta$ in the cost function in (16). To test this hypothesis, we simulated both the LSE and EBP optimizations with $Q = (I, 0; 0, 0)$

1/0.8	0.06/0.03	0.04/0.2	-0.01/0.1	0.001/0.001
-0.8/0.8	1/2	1/0.2	-0.4/-1	0.05/0.05
0.3/0.7	-0.2/-0.1	0.5/0.2	0.1/-0.1	-0.01/-0.01
-0.7/-0.1	0.5/0.6	1/0.8	0.7/0.4	0.03/0.03

TABLE I

MATRICES A (TOP) AND H (BOTTOM) OF THE LINEAR DYNAMIC MODEL AS COMPUTED FOR THE TOY PROBLEM USING THE LSE AND EBP OPTIMIZATION METHODS, FORMATTED [RESULT FROM LSE]/[RESULT FROM EBP].

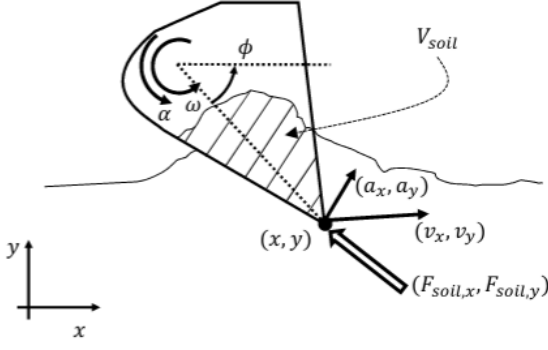


Fig. 6. Diagram of the states and physical observables included in the data.

to remove the penalty on $r_{\eta_t}^{\theta}$. The resulting A matrices were effectively equivalent. Importantly, these results indicate that the EBP optimization technique from § III is both less computationally expensive and more accurate than the LSE method.

V. APPLICATION TO EXCAVATION PROCESS MODELING

We also test the learned lifting linearization algorithm on an autonomous excavator simulation using *agxTerrain*, a specialized module of the AGX Dynamics [31] physics simulator used to test algorithms for autonomous excavation [32]–[34] illustrated in Fig. 1. We generate a random soil profile by summing several 2-D Gaussians of random height and variance, yielding soil shapes like those in Fig. 1. Soil properties are set in accordance to the AGX “gravel” profile.

Using the software, we collect 100 7.5s trajectories at 100Hz. A diagram of the collected data is illustrated in Fig. 6. The trajectories include six states, x : position along the x -axis, x ; position along the y -axis, y ; bucket angle, ϕ ; velocity along the x -axis, \dot{x} ; velocity along the y -axis, \dot{y} ; and rotational velocity of the bucket, ω .

The trajectories also include three control inputs, u : force along the x -axis, u_x ; force along the y -axis, u_y ; and torque actuating the bucket, u_ϕ .

The trajectories also include six physical observables, ζ : acceleration of the bucket tip along the x -axis, a_x ; acceleration of the bucket tip along the y -axis, a_y ; rotational acceleration of the bucket, α ; soil reaction force at the bucket tip along the x -axis, F_x ; soil reaction force at the bucket tip along the y -axis, F_y ; and volume of the soil in the bucket, V_{soil} .

These trajectories are generated using a naïve, noisy PID controller on the translation forces and bucket angle:

$$\begin{aligned} u_x &= \text{PID}(\dot{x} - \mathcal{U}(\dot{x}_{\min}, \dot{x}_{\max})) + \mathcal{U}(-w_x, w_x) \\ u_y &= \text{PID}(\dot{y} - \mathcal{U}(\dot{y}_{\min}, \dot{y}_{\max})) + \mathcal{U}(-w_y, w_y) \\ u_\phi &= \text{PID}(\phi - \mathcal{U}(\phi_{\min}, \phi_{\max})) + \mathcal{U}(-w_\phi, w_\phi) \end{aligned} \quad (27)$$

where \mathcal{U} is the uniform random distribution. The set points are drawn from a uniform random distribution in accordance with [35].

The learned lifting linearization and Koopman models for the terramechanics experiment are almost identical to

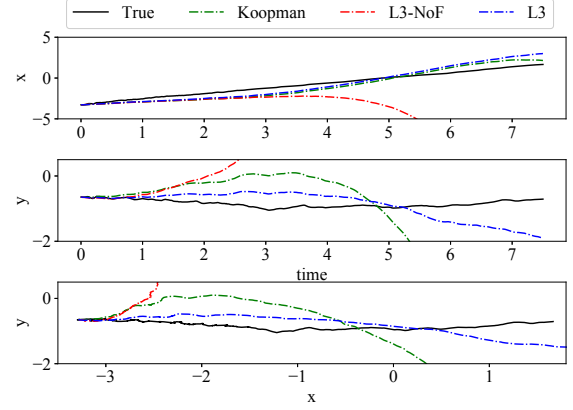


Fig. 7. Results of simulation predicting the x and y trajectories of the bucket through the soil given the initial condition and control input. The solid black line indicates the true, observed trajectory. The dashed green line indicates the trajectory predicted by the Koopman model. The dashed blue line indicates the trajectory predicted by the learned lifting linearization (L3). The dashed red line indicates the trajectory predicted by the learned lifting linearization without first filtering out the control input using (25).

those of the nonlinear mass-spring-damper experiment, with some exceptions. The neural network, g , has 15 linear input neurons and 7 linear output neurons. Before training, one trajectory is set aside to be used for testing, and the remaining data are randomly divided 80-20 into a training set and a validation set. The batch size used for training the learned lifting linearization model is 32. The Adam optimizer used for training the learned lifting linearization model has a learning rate of $\alpha = 10^{-5}$. The domain of the Koopman dynamic model has a dimensionality of 32, compared to 22 for the learned lifting linearization model.

In addition to benchmarking the learned lifting linearization model against the Koopman model, we also compare the results with and without filtering out the control input from the physical observables using (25). In this model, instead of following the procedure described in § III-B, we incorporated $\zeta(x, u)$ directly into the state without filtering. Effectively, this forces the model to violate causality by predicting future values of observables dependent upon control input, u .

After training the learned lifting linearization and Koopman models, we simulate both models using the control input trajectory and initial condition from the testing trajectory. The modeled trajectories of the first two states, x and y , are compared against the ground truth in Fig. 7. The sum squared error across all six states for the learned lifting linearization model is only 6% of the same error for the Koopman model.

Separately, we retrain the learned lifting linearization model *without* first filtering out the control input using (25) and simulate using the same technique. The simulation quickly diverges from the ground truth. The sum squared error across all six states is more than 100 times the same error for the Koopman model. Clearly, input filtering is vital to model robustness.

VI. CONCLUSION

In this paper, we presented a learned lifting linearization algorithm to model nonlinear dynamic systems. This model extended Koopman operator theory and dual faceted linearization by training a neural network to produce nonlinear observables to augment the state. We also presented an algorithm to “clean” anticausal physical observables of any linear dependence on control input so that they can be used by the neural network to generate richer synthetic observables. We tested this algorithm on a nonlinear mass-spring-damper model and an autonomous excavation simulation, and we compared the results against Koopman and DFL models. In both cases, learned lifting linearization outperformed both Koopman operators and DFL at minimizing state prediction error. Furthermore, the input-filtering algorithm proved essential to producing valid results.

REFERENCES

- [1] S. Dadhich, U. Bodin, and U. Andersson, “Key challenges in automation of earth-moving machines,” *Automation in Construction*, vol. 68, pp. 212–222, 2016.
- [2] F. Ng, J. A. Harding, and J. Glass, “An eco-approach to optimise efficiency and productivity of a hydraulic excavator,” *Journal of cleaner production*, vol. 112, pp. 3966–3976, 2016.
- [3] R. Fukui, T. Niho, M. Nakao, and M. Uetake, “Imitation-based control of automated ore excavator: improvement of autonomous excavation database quality using clustering and association analysis processes,” *Advanced Robotics*, vol. 31, no. 11, pp. 595–606, 2017.
- [4] O. Luengo, S. Singh, and H. Cannon, “Modeling and identification of soil-tool interaction in automated excavation,” in *Proceedings. 1998 IEEE/RSJ International Conference on Intelligent Robots and Systems. Innovations in Theory, Practice and Applications (Cat. No. 98CH36190)*, vol. 3, pp. 1900–1906, IEEE, 1998.
- [5] R. J. Sandzimier and H. H. Asada, “A data-driven approach to prediction and optimal bucket-filling control for autonomous excavators,” *IEEE Robotics and Automation Letters*, vol. 5, no. 2, pp. 2682–2689, 2020.
- [6] F. E. Sotiropoulos and H. H. Asada, “A model-free extremum-seeking approach to autonomous excavator control based on output power maximization,” *IEEE Robotics and Automation Letters*, vol. 4, no. 2, pp. 1005–1012, 2019.
- [7] I. Abraham and T. D. Murphey, “Active learning of dynamics for data-driven control using koopman operators,” *IEEE Transactions on Robotics*, vol. 35, no. 5, pp. 1071–1083, 2019.
- [8] D. Bruder, B. Gillespie, C. D. Remy, and R. Vasudevan, “Modeling and control of soft robots using the koopman operator and model predictive control,” *arXiv preprint arXiv:1902.02827*, 2019.
- [9] A. Broad, T. Murphey, and B. Argall, “Learning models for shared control of human-machine systems with unknown dynamics,” *arXiv preprint arXiv:1808.08268*, 2018.
- [10] Y. Susuki, I. Mezić, F. Raak, and T. Hikiyara, “Applied koopman operator theory for power systems technology,” *Nonlinear Theory and Its Applications, IEICE*, vol. 7, no. 4, pp. 430–459, 2016.
- [11] A. Leonard, J. Rogers, and A. Gerlach, “Koopman operator approach to airdrop mission planning under uncertainty,” *Journal of Guidance, Control, and Dynamics*, vol. 42, no. 11, pp. 2382–2398, 2019.
- [12] M. Zhang, S. Vikram, L. Smith, P. Abbeel, M. Johnson, and S. Levine, “Solar: Deep structured representations for model-based reinforcement learning,” in *International Conference on Machine Learning*, pp. 7444–7453, PMLR, 2019.
- [13] B. Ichter and M. Pavone, “Robot motion planning in learned latent spaces,” *IEEE Robotics and Automation Letters*, vol. 4, no. 3, pp. 2407–2414, 2019.
- [14] T. Haarnoja, A. Ajay, S. Levine, and P. Abbeel, “Backprop kf: Learning discriminative deterministic state estimators,” *arXiv preprint arXiv:1605.07148*, 2016.
- [15] M. Watter, J. T. Springenberg, J. Boedecker, and M. Riedmiller, “Embed to control: A locally linear latent dynamics model for control from raw images,” *arXiv preprint arXiv:1506.07365*, 2015.
- [16] A. Mauroy, Y. Susuki, and I. Mezić, *The Koopman Operator in Systems and Control*. Springer, 2020.
- [17] H. Harry Asada and F. E. Sotiropoulos, “Dual faceted linearization of nonlinear dynamical systems based on physical modeling theory,” *Journal of Dynamic Systems, Measurement, and Control*, vol. 141, no. 2, 2019.
- [18] M. Korda and I. Mezić, “Linear predictors for nonlinear dynamical systems: Koopman operator meets model predictive control,” *Automatica*, vol. 93, pp. 149–160, 2018.
- [19] B. O. Koopman, “Hamiltonian systems and transformation in hilbert space,” *Proceedings of the national academy of sciences of the united states of america*, vol. 17, no. 5, p. 315, 1931.
- [20] S. Maćešić and N. Črnjarić-Žic, “Koopman operator theory for nonautonomous and stochastic systems,” in *The Koopman Operator in Systems and Control*, pp. 131–160, Springer, 2020.
- [21] I. Mezić, “Analysis of fluid flows via spectral properties of the koopman operator,” *Annual Review of Fluid Mechanics*, vol. 45, pp. 357–378, 2013.
- [22] M. Budišić, R. Mohr, and I. Mezić, “Applied koopmanism,” *Chaos: An Interdisciplinary Journal of Nonlinear Science*, vol. 22, no. 4, p. 047510, 2012.
- [23] J. H. Tu, C. W. Rowley, D. M. Luchtenburg, S. L. Brunton, and J. N. Kutz, “On dynamic mode decomposition: Theory and applications,” *arXiv preprint arXiv:1312.0041*, 2013.
- [24] Y. Igarashi, M. Yamakita, J. Ng, and H. H. Asada, “Mpc performances for nonlinear systems using several linearization models,” in *2020 American Control Conference (ACC)*, pp. 2426–2431, IEEE, 2020.
- [25] F. E. Sotiropoulos and H. H. Asada, “Causality in dual faceted linearization of nonlinear dynamical systems,” in *2018 Annual American Control Conference (ACC)*, pp. 1230–1237, IEEE, 2018.
- [26] Y. Han, W. Hao, and U. Vaidya, “Deep learning of koopman representation for control,” in *2020 59th IEEE Conference on Decision and Control (CDC)*, pp. 1890–1895, IEEE, 2020.
- [27] G. Mamakoukas, M. Castano, X. Tan, and T. Murphey, “Local koopman operators for data-driven control of robotic systems,” in *Robotics: science and systems*, 2019.
- [28] A. Paszke, S. Gross, F. Massa, A. Lerer, J. Bradbury, G. Chanan, T. Killeen, Z. Lin, N. Gimelshein, L. Antiga, A. Desmaison, A. Kopf, E. Yang, Z. DeVito, M. Raison, A. Tejani, S. Chilamkurthy, B. Steiner, L. Fang, J. Bai, and S. Chintala, “Pytorch: An imperative style, high-performance deep learning library,” in *Advances in Neural Information Processing Systems 32* (H. Wallach, H. Larochelle, A. Beygelzimer, F. d’Alché-Buc, E. Fox, and R. Garnett, eds.), pp. 8024–8035, Curran Associates, Inc., 2019.
- [29] N. S. Selby, “Dfl,” <https://github.com/rupumped/DFL>, 2021.
- [30] D. P. Kingma and J. Ba, “Adam: A method for stochastic optimization,” *arXiv preprint arXiv:1412.6980*, 2014.
- [31] Algoryx, “Agx dynamics,” <https://www.algoryx.se/agx-dynamics/>. Accessed: 2021-02-24.
- [32] Y. Yang, J. Pan, P. Long, X. Song, and L. Zhang, “Time variable minimum torque trajectory optimization for autonomous excavator,” *arXiv preprint arXiv:2006.00811*, 2020.
- [33] Y. Yang, L. Zhang, X. Cheng, J. Pan, and R. Yang, “Compact reachability map for excavator motion planning,” in *2019 IEEE/RSJ International Conference on Intelligent Robots and Systems (IROS)*, pp. 2308–2313, IEEE, 2019.
- [34] S. Ulin, “Digging deep: A data-driven approach to model reduction in a granular bulldozing scenario,” 2018.
- [35] J. L. Proctor, S. L. Brunton, and J. N. Kutz, “Generalizing koopman theory to allow for inputs and control,” *SIAM Journal on Applied Dynamical Systems*, vol. 17, no. 1, pp. 909–930, 2018.